27

Numerical Simulations of the Long-Haul RZ-DPSK Optical Fibre Transmission System

Hidenori Taga
National Sun Yat-Sen University
Taiwan

1. Introduction

Return-to-zero differential phase shift keying (RZ-DPSK) is a promising modulation format for the long-haul large capacity optical fibre transmission system, and it demonstrated a superior performance compared to the conventional intensity-modulation direct-detection (IM-DD) system experimentally (Cai et al., 2006; Inoue et al., 2004; Rasmussen et al., 2004). For the IM-DD based long-haul system, dispersion map is a commonly used technology to improve the transmission performance (Bergano, 2005). The dispersion map was developed to compromise following two incompatible conditions: close to zero dispersion is preferred from the point of the waveform distortion due to the chromatic dispersion, while a finite dispersion is required to reduce the nonlinear degradation due to the optical fibre. The dispersion map realizes close to zero end-to-end dispersion while keeping the finite local dispersion by combining positive and negative dispersion fibre in the transmission line. For example, the positive dispersion fibre is a standard single mode fibre (SMF), and the negative dispersion fibre is a non-zero dispersion shifted fibre (NZDSF). For the long-haul IM-DD system, so-called "block type" dispersion map is the most popular style. For this block type dispersion map, both the positive and negative dispersion fibres are combined to compose one dispersion block of several hundred to one thousand kilometres, and an entire long-haul system is composed of several dispersion blocks (Bergano, 2005).

Even though the block type dispersion map is effective to improve the performance of the conventional IM-DD based system, it was reported that the performance of the long-haul 10Gbit/s RZ-DPSK system with the block type dispersion map using the NZDSF and the SMF showed performance degradation near the system zero dispersion wavelength (Dupont et al., 2007; Moh et al., 2007; Vaa et al., 2004). It is a strange feature of the RZ-DPSK transmission system, because the conventional IM-DD system shows better performance near the system zero dispersion wavelength rather than the other wavelengths. Then, this chapter has been intended to clarify the reason why the long-haul RZ-DPSK system shows such behaviour using the numerical simulations.

Section 2 describes the method of the numerical simulations. The simulator is using the standard calculation scheme of the long-haul optical fibre transmission. It solves the nonlinear Schrödinger equation using the split-step Fourier method (Agrawal, 2006). Using this simulator, the transmission performance of the long-haul RZ-DPSK system is evaluated, and the difference between the block type and block-less type maps is compared in section 3. The results obtained through the simulation agree to the experimental results

qualitatively, and the validity of the simulation program is confirmed (Taga, 2007). In section 4, a little more detail of the transmission performance of the block type dispersion map is investigated. By reducing number of the dispersion blocks in the system, the performance is simulated, and it is confirmed that smaller number of the dispersion blocks improves the system performance without changing any system parameters (Taga, 2008). In section 5 and 6, the transmission performance of the long-haul RZ-DPSK system using an advanced optical fibre is simulated. For the IM-DD based long-haul system, the dispersion flattened fibre (DFF) is developed to improve the transmission performance, and it was already installed in the Pacific Ocean (Bakhshi, 2004). The DFF should also be effective to improve the transmission performance of the RZ-DPSK based system, and a comparison of the long-haul system using the conventional NZDSF and the DFF is conducted (Taga, 2009). The difference between the block type and block-less type dispersion map using the DFF is also investigated (Taga & Chung, 2010). Finally, this chapter is concluded.

2. Simulation method

There are various methods for the numerical simulation of the optical pulse propagation. For the simulation of the optical fibre communication system, optical pulse propagation described by the nonlinear Schrödinger equation should be calculated, and the split-step Fourier method is generally used for the calculation (Agrawal, 2006). In this section, the simulation technique using the split-step Fourier method is briefly explained.

2.1 Split-step Fourier calculation

The numerical simulator solved the coupled nonlinear Schrödinger equations using the split-step Fourier method. The equation used for the simulation is

$$\frac{\partial A_j}{\partial z}+\frac{i}{2}\beta_{2j}\frac{\partial^2 A_j}{\partial T^2}-\frac{\beta_{3j}}{6}\frac{\partial^3 A_j}{\partial T^3}+\frac{\alpha_j}{2}A_j=i\gamma_j\left(\left|A_j\right|^2+2\sum_{k\neq j}\left|A_k\right|^2\right)A_j \tag{1}$$

where A is the amplitude of the electrical field of the optical signal, z is the distance in the fibre, T is the time, β_2 is the second-order group velocity dispersion (GVD) coefficient, β_3 is the third-order GVD coefficient, α is the fibre loss coefficient, γ is the nonlinear parameter of the fibre, and the subscripts j and k are the channel number. The split-step Fourier method calculates this equation through two steps. The first step calculates the linear part while ignoring the nonlinear terms. As the linear part contains partial differentiations, the calculation utilizes the Fourier transform to convert the differentiations in the time domain into the frequency multiplications in the frequency domain. Using the Fourier transform and inverse Fourier transform, the partial differentiations are calculated in the frequency domain and converted back to the time domain. The second step calculates the nonlinear part while ignoring the linear terms. Repeating these two steps, the optical pulse propagation within the optical fibre can be calculated numerically.

It is known that the sprit-step method generates spurious tones in the frequency domain if the step length is set uniform (Bosco et al., 2000). Therefore, the fibre step length for the split-step calculation was set to nonuniform, and it was expanded exponentially from the initial length of 100 metres. The reason to expand the step length exponentially is the fact that the transmission loss of the fibre decays the optical signal power exponentially. Then,

the product of the signal power and the fibre step length becomes constant, and it could maintain the effect of the fibre nonlinearity in each calculation step.

2.2 Q-factor calculation

In general, transmission performance of the digital communication system is evaluated by the bit-error rate (BER). The optical fibre communication system is no exception. Therefore, the numerical simulation needs a functionality to evaluate the transmission performance by the BER. A Monte-Carlo scheme is the straightforward way to evaluate the BER, but it requires large number of simulated bits to evaluate small BER. It takes long time to simulate large number of bits, and the Monte-Carlo method is not efficient to obtain small BER values. Then, a Q-factor is calculated through the simulation to evaluate the transmission performance. The definition of the Q-factor is (Personick, 1973)

$$Q = \frac{|\mu_1 - \mu_0|}{\sigma_1 + \sigma_0} \tag{2}$$

where μ_1 and μ_0 are the averaged value of "1" bits and "0" bits, respectively, and σ_1 and σ_0 are the standard deviation of "1" bits and "0" bits, respectively. Fig. 1 shows the relationship of these parameters and the intensity eye diagram of the received optical signal schematically. The Q-factor is related to the BER through the equation

$$BER = \frac{1}{2} erfc\left(\frac{Q}{\sqrt{2}}\right) \tag{3}$$

Therefore, it is possible to obtain the BER from the Q-factor. As a matter of fact, the Q-factor is widely used for evaluating the transmission performance of the optical fibre communication system (Bergano et al., 1993).

For the DPSK system, however, it is impossible to obtain the intensity eye diagram like shown in Fig. 1 through the numerical simulation. Therefore, a method to use the phase eye diagram to calculate the Q-factor was proposed (Wei et al., 2003). For this scheme, the optical signal phase is directly calculated from the optical field. The difference of the phase is defined as the phase difference between two sampling points separated by one bit period, and it is plotted between $3\pi/2$ and $-\pi/2$. Then, the averaged value and the standard

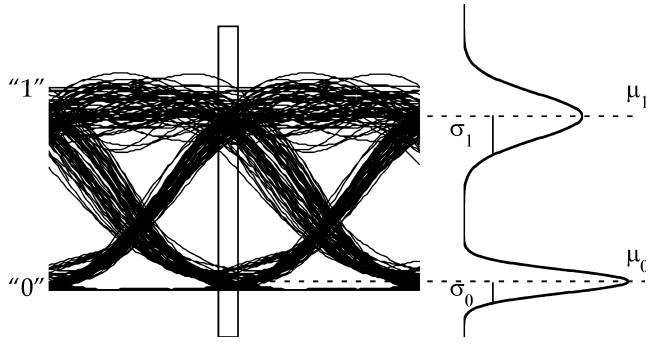

Fig. 1. Relationship of parameters and intensity eye diagram

deviation of "π" phase and "0" phase can be calculated. The Q-factor can be defined similar to equation (2) as

$$Q = \frac{|\mu_\pi - \mu_0|}{\sigma_\pi + \sigma_0} \tag{4}$$

where μ_π and μ_0 are the averaged value of "π" phase bits and "0" phase bits, respectively, and σ_π and σ_0 are the standard deviation of "π" phase bits and "0" phase bits, respectively. Fig. 2 shows the relationship of these parameters and the phase eye diagram of the received optical signal schematically. Using this Q-factor, it becomes possible to estimate the transmission performance of the simulated DPSK system.

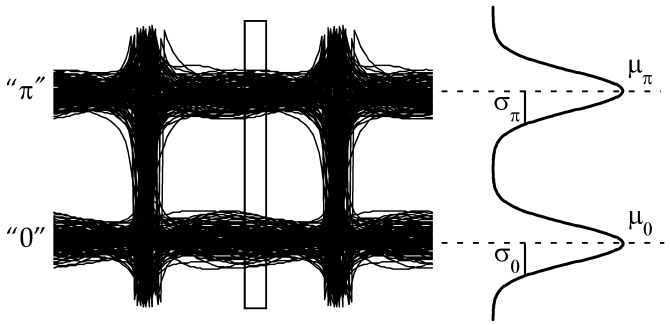

Fig. 2. Relationship of parameters and phase eye diagram

3. Comparison of block type and block-less type dispersion map

The long-haul RZ-DPSK transmission system showed significantly different behaviour between the block type dispersion map and the block-less type dispersion map (Dupont et al., 2007; Moh et al., 2007; Vaa et al., 2004). It is important to clarify the reason why the RZ-DPSK transmission system showed such behaviour. Numerical simulations have been conducted to clarify this issue.

3.1 Simulation model

Fig. 3 shows a schematic diagram of the simulation model. Thirty-two optical transmitters (TXs) with the signal wavelengths ranged between 1543.8 to 1556.2 nm were used. The channel separation was set to 0.4 nm. The bit rate and the pattern of the transmitters were 10 Gb/s and 2^9 De Brujin sequence, respectively. A Mach–Zehnder modulator (MZM) was assumed to generate the PSK signal, and the waveform applied for the two arms of the MZM was a raised cosine with the non-return-to-zero (NRZ) format. The RZ waveform was applied after the PSK modulation, and the waveform was also raised cosine. The pulse duty ratio was 50 %. The multiplexer (MUX) did not have any wavelength-selective function, and the modulated pattern of each transmitter was randomized at the output of the MUX. Three different sets of the initial pattern at the output of the MUX was simulated in order to reduce the pattern-dependent cross phase modulation (XPM) impact (Essiambre & Winzer, 2005), and the obtained results were averaged over these three sets.

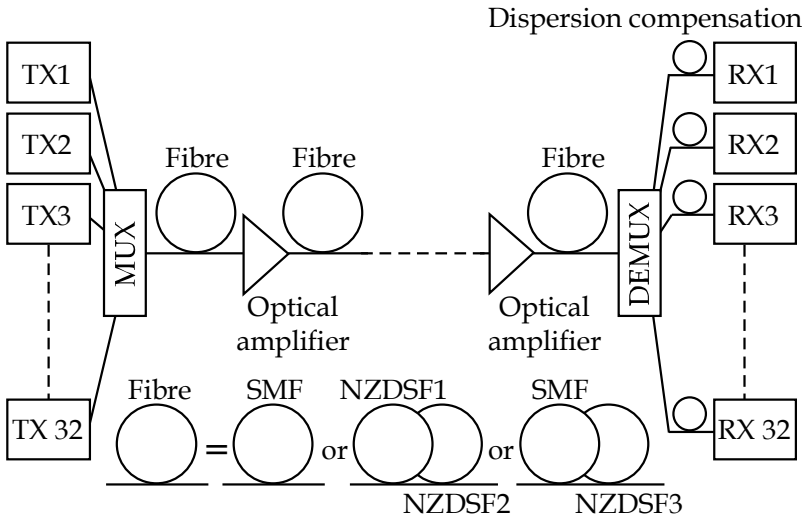

Fig. 3. A schematic diagram of the simulation model

The output power and the noise figure of the optical amplifier repeater were set to +11 dBm and 4.5 dB, respectively. The amplifier spontaneous emission (ASE) noise generated by the repeater had a random complex electrical field, and it was added to the complex electrical field of the optical signal. The repeater span length was 100 km, and the number of the repeaters was 63. The wavelength-dependent gain of the repeater was ignored in the simulation.

The optical demultiplexer (DEMUX) had the first-order Gaussian shape with the bandwidth of 0.1 nm. The cumulative chromatic dispersion for each channel was compensated at the receiving end, and the residual dispersion after dispersion equalization was set to 100 ps/nm. The Q-factor was calculated for each channel.

Two different dispersion maps were simulated. The first one was the conventional block type dispersion map, and the second one was the block-less type map. Both maps used the NZDSF and the SMF, but the parameters of the fibres were slightly different for each map. Table 1 summarizes the parameters of those fibres (Moh et al., 2007). The block type map comprised eight NZDSF spans and one SMF span to compose one block, and the SMF span was placed in the centre of the block (i.e., fifth span). Each NZDSF span comprised NZDSF1 and NZDSF2. The differences of these two fibres were the effective area and the dispersion slope. The block-less type map comprised hybrid spans except for both ends of the transmission line. The hybrid span was composed of the SMF and the NZDSF, while only the SMFs were used for both ends. Fig. 4 shows the cumulative dispersion at 1550 nm of these two maps. While the block type map compensated the cumulative dispersion periodically, the block-less type map compensated the cumulative dispersion only at both ends. The averaged zero dispersion wavelength of both maps was set to 1550 nm, and the transmission distances were 6300 km for the block type map and 6360 km for the block-less type map.

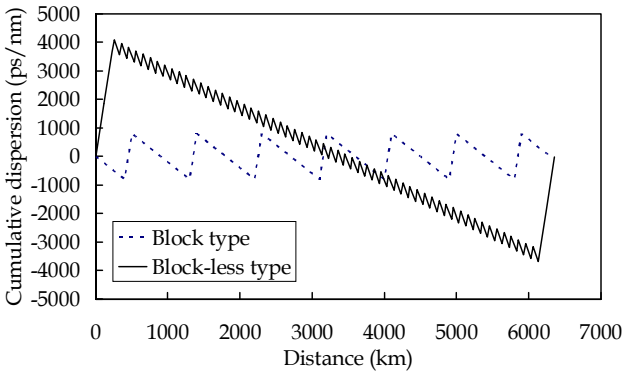

Fig. 4. Dispersion maps of the simulated systems

	Block type			Block-less type	
	NZDSF1	NZDSF2	SMF	SMF	NZDSF3
Length (km)	50	50	100	25	75
Loss (dB/km)	0.21	0.21	0.18	0.18	0.21
Chromatic dispersion (ps/nm/km)	-2.0	-2.0	16.0	16.0	-7.0
Dispersion slope (ps/nm^2/km)	0.10	0.06	0.06	0.06	0.08
Effective area (≅m^2)	70	50	100	100	50
Nonlinear refractive index	2.6×10^{-20}				

Table 1. Fibre parameters used for the simulation

3.2 Simulation results

Fig. 5 shows a comparison of two dispersion maps. The obtained Q-factors are shown as a function of the signal channels. For the block type map, the Q-factor is degraded near the centre channels, while there is not a significant dependence upon the channels for the block-less type map. The averaged Q-factors were 12.3 and 13.7 dB for the block type map and the block-less type map, respectively. These results qualitatively agree the experimental result (Moh et al., 2007) because it showed a performance dip near the centre channels for the block type map and the performance improvement for the block-less type map.

Then, to examine the reason of the performance improvement of the block-less type map, the effects of the self phase modulation (SPM) and the XPM were evaluated. Fig. 6 (A) and (B) show the performance without the SPM or the XPM of the block type map and the block-less type map, respectively. As shown in Fig. 6 (A), the performance of the block type map was greatly improved when the SPM was ignored especially near the centre channels, while the improvement was small when the XPM was ignored. From this result, it can be said that the SPM caused the performance degradation near the centre wavelength channels of the block type map. On the other hand, as shown in Fig. 6 (B) for the case of the block-less type map, the performance improvement caused by ignoring the SPM was limited compared to the block type map, and the improvement was not channel dependent. In addition, the performance was almost identical when the XPM was ignored. The averaged Q-factors

without the SPM for the block type map and the block-less type map were 13.8 and 14.6 dB, respectively. The averaged Q-factors without the XPM for the block type map and the block-less type map were 12.9 and 13.7 dB, respectively

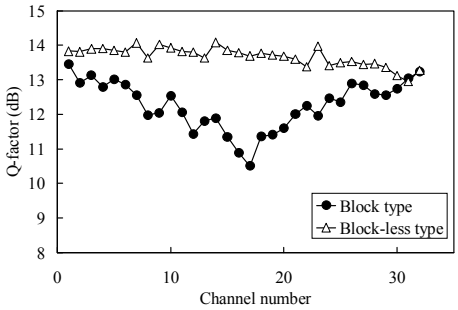

Fig. 5. Simulated transmission performance of the block type and block-less type map

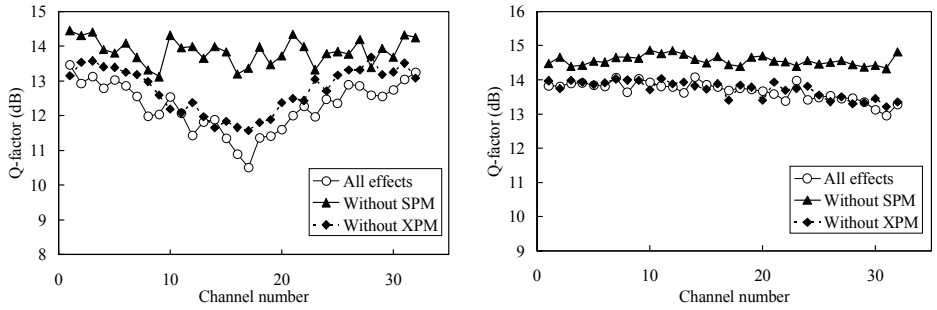

(A) Block type (B) Block-less type

Fig. 6. Impact of the SPM and XPM for the block type and block-less type map

Two conclusions can be drawn from these results. The first conclusion is the SPM causes the wavelength-dependent degradation for the block type map, and the degradation is significant in the region close to the system zero dispersion wavelength. The second conclusion is the XPM plays a relatively minor role of the performance degradation of the block type map while it has virtually no effect for the block-less type map. It can be concluded that the block-less type dispersion map reduces the impairments of both the SPM and the XPM for the long-haul RZ-DPSK transmission compared to the block type dispersion map, and improves the system performance.

4. Impact of number of dispersion blocks

Comparing the block type map and the block-less type map, one notable difference between them is number of zero-crossing points of the cumulative dispersion along the transmission distance. This is due to number of dispersion blocks in the system. Therefore, in this section, the effect of number of dispersion blocks upon the transmission performance of the long-

haul RZ-DPSK system is studied. At first, the system performance of the block type dispersion map was evaluated as a function of the transmission distance. Then, the system performances of several different block type dispersion maps were evaluated as a function of number of dispersion blocks in the system.

4.1 Simulated dispersion maps

The model used for this study was the same as the previous study, and it is shown in Fig. 3. The simulated block type dispersion maps were using NZDSF1, NZDSF2, and SMF shown in Table 1. The output power and the noise figure of the optical amplifier repeater were set to +11 dBm and 4.5 dB, respectively. The repeater span length was 100km, and the total transmission distance was 6300 km.

Number of dispersion blocks was adjusted by changing the position of the SMF span in the transmission line. Then, different style of the dispersion maps was realized whereas the fibre parameters were kept identical. Fig. 7 shows these maps. Number of dispersion blocks was one to seven corresponding to the number of dispersion map. This means Map 1 has one dispersion block, Map 2 has two dispersion blocks, and so on.

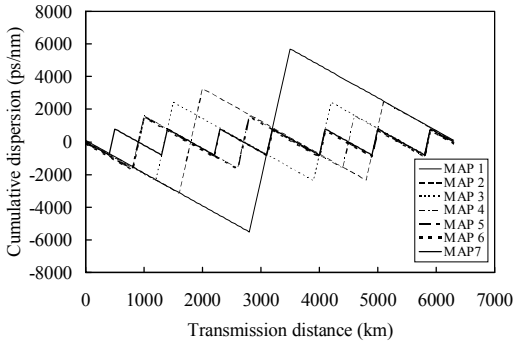

Fig. 7. Dispersion maps with different number of dispersion blocks

4.2 Transmission distance dependency

At first, the system performance of Map 7 was evaluated as a function of the transmission distance. Fig. 8 shows the results. The horizontal axes shows the channel number, and the vertical axes shows the relative Q-factor for each transmission distance. The relative Q-factor is defined as the difference from the value of channel 32. As seen in this figure, the performance dip near the system zero dispersion wavelength became obvious when the transmission distance was increased. This tendency implies that large number of dispersion blocks causes the performance degradation near the system zero dispersion wavelength. Then, the effects of the SPM and the XPM were investigated. Fig. 9 (A) and (B) show the transmission distance dependency without the SPM and the XPM, respectively. As shown in Fig. 9 (A), there is not any significant dip when the SPM effect was ignored, while the degradation near the centre channels was obvious for Fig. 9 (B). These results imply that large number of dispersion blocks combined with the SPM degrades the performance of the RZ-DPSK signal near the system zero dispersion wavelength.

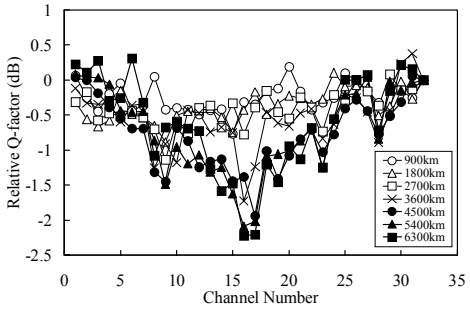

Fig. 8. Relative channel performance as a function of the transmission distance

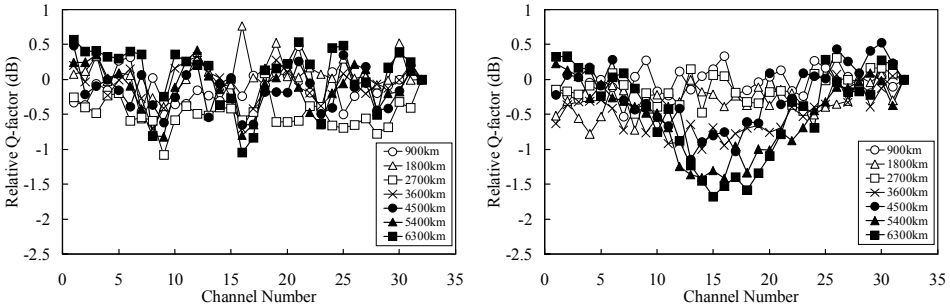

(A) without the SPM (B) without the XPM

Fig. 9. Relative channel performance as a function of the transmission distance without the SPM and the XPM

4.3 Number of dispersion blocks dependency

Next, the system performance of several different block type dispersion maps shown in Fig. 7 was evaluated. Fig. 10 shows the results. As seen in the figure, the performance dip near

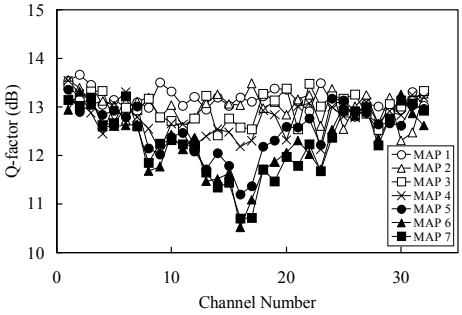

Fig. 10. Transmission performance of different number of dispersion blocks

the centre channels became significant when number of dispersion blocks was increased. This tendency clearly shows that large number of dispersion blocks causes the performance degradation near the system zero dispersion wavelength. Then, the effects of the SPM and the XPM were investigated. Fig. 11 (A) and (B) show the dispersion map dependency without the SPM and the XPM, respectively. As shown in Fig. 11 (A), there is not any significant dip when the SPM effect was ignored, while the degradation near the centre channels was obvious for Fig. 11 (B). These results show that large number of dispersion blocks combined with the SPM degrades the performance of the RZ-DPSK signal near the system zero dispersion wavelength.

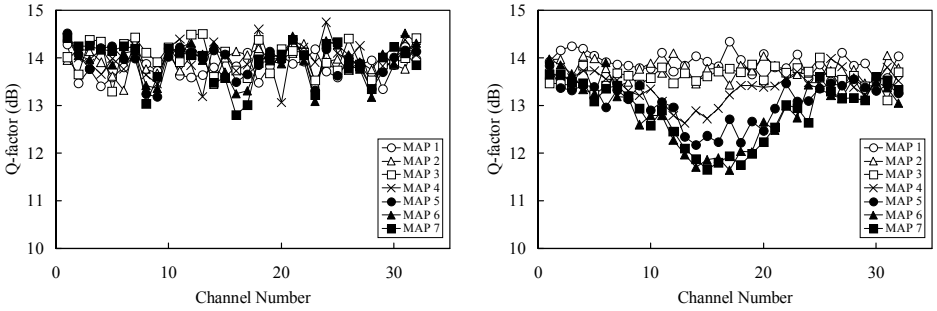

(A) without the SPM (B) without the XPM

Fig. 11. Transmission performance of different number of dispersion blocks without the SPM and the XPM

5. Comparison of dispersion flattened fibre and non-zero dispersion shifted fibre

The DFF is a well-known solution to improve the performance of the long-haul IM-DD system, but there are not enough studies to characterize the transmission performance difference between the DFF and the NZDSF for the RZ-DPSK based system. In this section, a comparative study of the long-haul RZ-DPSK system performance using the DFF and the NZDSF is conducted.

5.1 Simulation model

Fig. 12 shows a schematic diagram of the simulation model. Ninety-six optical TXs were employed, and the signal wavelengths were ranged from 1540.5 nm to 1559.5 nm with 0.2 nm channel separation. The bit rate and the pattern were 10 Gbit/s and 2^9 De Brujin sequence, respectively. The PSK signal was assumed to be generated by a MZM, and the waveform applied for the two arms of the MZM was a raised cosine with the NRZ format. The RZ waveform was applied after the PSK modulation, and the waveform was also raised cosine. The pulse duty ratio was 50 %. The MUX did not have any wavelength selective function, and the modulated pattern of each transmitter was randomized at the output of the MUX. Three different sets of the initial pattern at the output of the MUX were used for the simulation to reduce the pattern dependent XPM impact (Essiambre & Winzer, 2005), and the obtained results were averaged over these three sets.

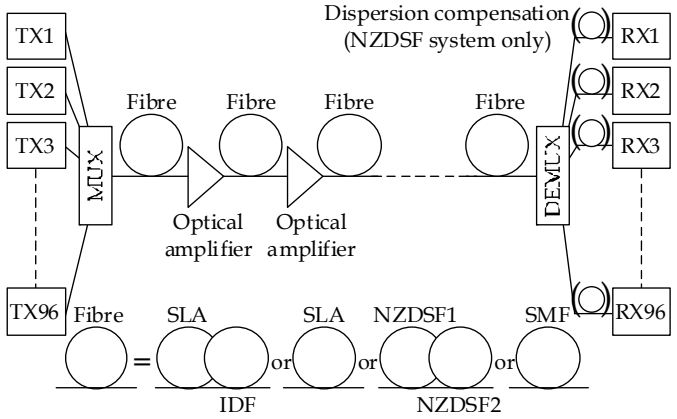

Fig. 12. A schematic diagram of the simulation model

The optical DEMUX had the second-order Gaussian shape, and the 3dB bandwidth of the DEMUX was 0.1 nm. As the relative dispersion slope of the SLA and the IDF was the same, the cumulative dispersion of all signal channels after the transmission was equal to zero for the DFF system. On the other hand, the cumulative dispersion of each channel was equalized to be 100 ps/nm for the NZDSF system after the DEMUX.

The transmission line comprised optical amplifier repeaters and fibres. The noise figure of the optical amplifier repeater was set to 4.5 dB. The ASE noise generated by the amplifier had a random complex electrical field, and it was added to the complex electrical field of the optical signal. The amplifier spacing was 100 km. The wavelength dependent gain of the optical amplifier was ignored in the simulation.

The fibre span comprised the DFF or the NZDSF. The DFF was composed from the super large area fibre (SLA) and the inverse dispersion fibre (IDF) (OFS), and there were two types of the NZDSF. The parameters of the fibres are summarized in Table 2. The DFF span loss was 21.1 dB and the NZDSF span loss was 21.0 dB. Fig. 13 shows the dispersion map of the DFF system and the NZDSF system. The block-less type map was employed. Three different wavelengths, 1540.5, 1550, and 1559.5 nm were shown in the figure to show the difference between the fibres clearly. Both maps had pure positive fibre spans in the centre of the system, and the span length of this section was 96 km for the DFF system and 100 km for the NZDSF system. Thus, the total transmission distance was 6272 km and 6300 km for

	DFF		NZDSF		
	SLA	IDF	NZDSF1	NZDSF2	SMF
Length (km)	65	35	50	50	100
Loss (dB/km)	0.19	0.25	0.21	0.21	0.18
Chromatic dispersion (ps/nm/km)	20.0	-44.0	-2.0	-2.0	16.0
Dispersion slope (ps/nm^2/km)	0.06	-0.132	0.10	0.06	0.06
Effective area (m^2)	106	30	70	50	72
Relative dispersion slope	0.003	0.003	-	-	-
Nonlinear refractive index	2.6×10^{-20}				

Table 2. Fibre parameters of the DFF and the NZDSF

the DFF system and the NZDSF system, respectively. The positive dispersion fibre used for the DFF system was the SLA, and that for the NZDSF system was the SMF.

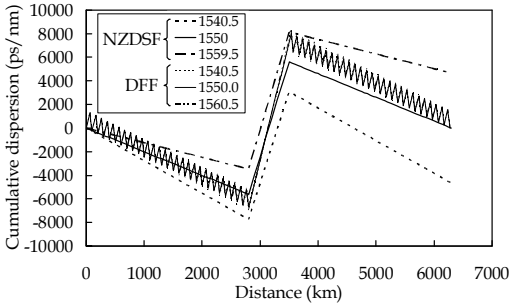

Fig. 13. Dispersion maps of the DFF and the NZDSF systems

5.2 Comparison of the dispersion flattened fibre and the non-zero dispersion shifted fibre based system

At first, the system performance was evaluated as a function of the repeater output power. Fig. 14 shows the results. The horizontal axis shows the repeater output power, and the vertical axis shows the averaged Q-factor of ninety-six channels. As seen in the figure, when the repeater output power was smaller than +14 dBm, the performance of both systems was similar. This result shows that the difference of the fibre parameters did not have so significant impact on the transmission performance when the optical fibre nonlinearity was not dominant. The performance was improved as the repeater output power was increased up to +18 dBm for the DFF system and up to +16 dBm for the NZDSF system. This result clearly shows that the DFF had smaller transmission impairment caused by the optical fibre nonlinearity than the NZDSF. When the repeater output power was +16 dBm, averaged Q-factors for the DFF system and the NZDSF system were 13.9 dB and 12.6 dB, respectively. There was 1.3 dB performance difference between the DFF and the NZDSF systems when the repeater output power was set to the optimum value of the NZDSF system. Furthermore, when the repeater output power was +18dBm, averaged Q-factor for the DFF system was improved to 14.9 dB. Therefore, the DFF system had 2.3 dB performance advantage against the NZDSF system when the system was operated under the optimum condition.

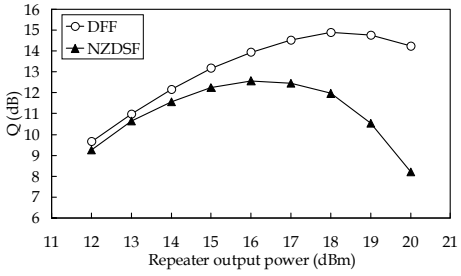

Fig. 14. Repeater output power dependency of the DFF and the NZDSF system

Fig. 15 shows channel dependence of the Q-factor for the DFF system and the NZDSF system. Fig. 15 (A) shows +14dBm repeater output power, and Fig. 15 (B) shows +16dBm repeater output power. The DFF system showed slightly improved performance than the NZDSF system in Fig. 15 (A), and it showed clearly better performance in Fig. 15 (B). In addition, Fig. 16 shows the comparison at the optimum repeater output power. The DFF system at +18 dBm repeater output power showed superior performance than the NZDSF system at +16 dBm. These results show that the DFF is effective to improve the transmission performance of the long-haul RZ-DPSK system, but the repeater output power should be high enough to fully utilize the advantage of the DFF.

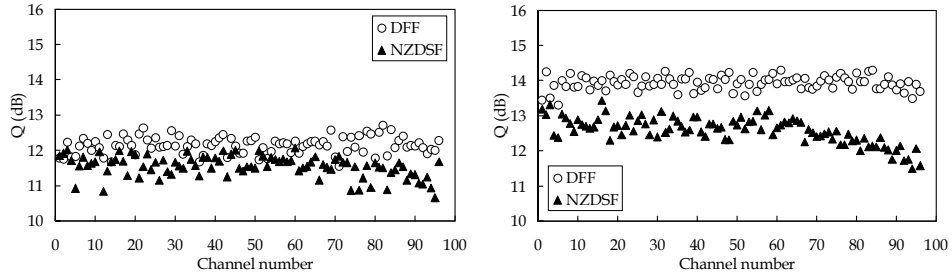

(A) +14 dBm repeater output power (B) +16 dBm repeater output power

Fig. 15. Transmission performance of 96 channels with the DFF and the NZDSF system

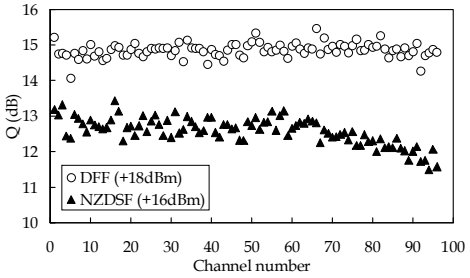

Fig. 16. Transmission performance of 96 channels with the optimum repeater output power

As mentioned above, the DFF system exhibited 2.3 dB performance improvement compared to the NZDSF system when the repeater output power was optimized. The reason of this 2.3 dB advantage could be explained in two steps. Firstly, there is 2 dB difference of the optimum repeater output power. This difference could be justified by the effective area difference between the SLA and NZDSF1. As the effective areas of the SLA and the NZDSF1 are 107 μm^2 and 70 μm^2, respectively, the difference of the effective area in dB scale is 1.8 dB, and this could cause 2 dB difference of the optimum power level. Roughly speaking, 2 dB improvement of the repeater output power improves the optical signal to noise ratio of 2 dB, and it can improve the Q-factor of 2 dB. Secondly, remaining 0.3dB discrepancy could be attributed to channel dependent degradation of the NZDSF

system at +16 dBm repeater output power. As shown in Fig. 15 (B), channel performance of the NZDSF system above the system zero dispersion wavelength clearly exhibits gradual degradation when the channel wavelength becomes longer. Actually, if the average Q-factor of the NZDSF system is calculated using only fourty-eight shorter wavelength channels (i.e., channel 1 to 48), the average is improved to 12.8 dB.

6. Impact of number of dispersion blocks for the dispersion flattened fibre based system

As discussed in section 4, for the NZDSF based system, the block type dispersion map is not optimum for the RZ-DPSK format and number of dispersion blocks changes the transmission performance significantly. This implies that the transmission performance of the DFF based system is also affected significantly by the number of dispersion blocks. Therefore, this section focuses on this issue whether the block type dispersion map causes the performance degradation of the DFF based RZ-DPSK system.

6.1 Simulation model

The simulation model used for this study was similar to that of the previous section, and it is shown in Fig. 12. The DFF parameters and span configuration was the same, and each DFF span had negative chromatic dispersion of -240ps/nm. The cumulative negative dispersion was compensated by the SLA only span. To compose the block type dispersion map, one dispersion block comprised nine DFF spans and one SLA only span. The SLA only span was placed at the sixth span. The span length of the SLA only span was 108km. There were six dispersion blocks, and the total transmission distance was 6048km.

Six different dispersion maps were used for the simulation. Number of dispersion blocks was changed for each map. Map 1 had one dispersion block, Map 2 had two dispersion blocks, and so on. Map 1, 2, 3, and 6 had uniform dispersion blocks while Map 4 and 5 had two different block lengths within the system. Fig. 17 shows the dispersion maps used for this study. Note that the difference was only the position of SLA only span, and the physical parameters of the fibres were identical.

6.2 Number of dispersion blocks dependency

Fig. 18 shows the performance of ninety-six channels after 6048km transmission as a function of the repeater output power. As seen in the figure, for small repeater output power of below +14 dBm, there was not any significant difference between the maps, but the performance of map 6 became inferior than the others when the repeater output power was increased above +16 dBm. These results clearly indicate that the nonlinear penalty of the system strongly depends on the dispersion map design.

Fig. 19 shows the average Q-factor of ninety-six channels as a function of the repeater output power and the dispersion map. It is obvious that increasing the number of dispersion blocks leads to performance degradation in higher repeater output power (i.e., higher nonlinear regime). Regarding dispersion map design, the tendency is the same as the NZDSF based system, and it is favourable for the DFF system to reduce number of dispersion blocks to improve the performance.

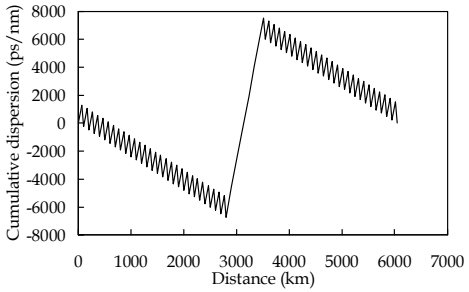

(A) Map 1

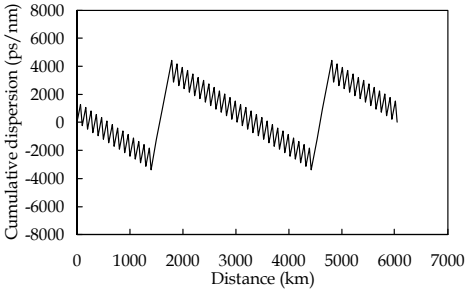

(B) Map 2

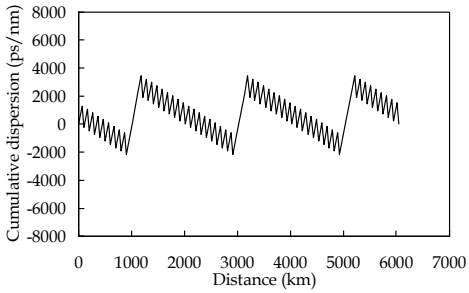

(C) Map 3

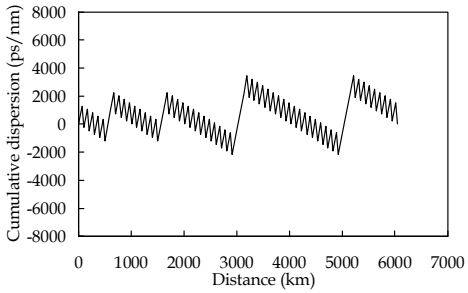

(D) Map 4

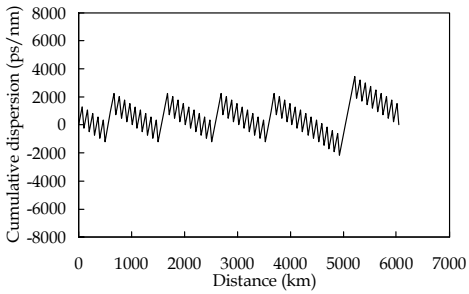

(E) Map 5

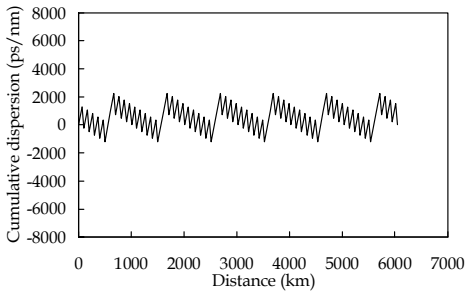

(F) Map 6

Fig. 17. Dispersion maps

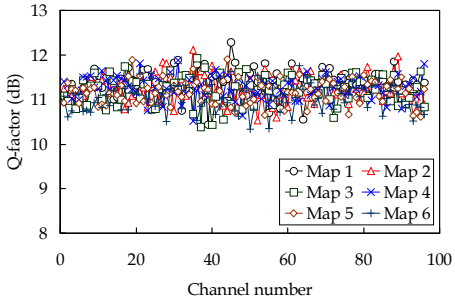

(A) +13 dBm

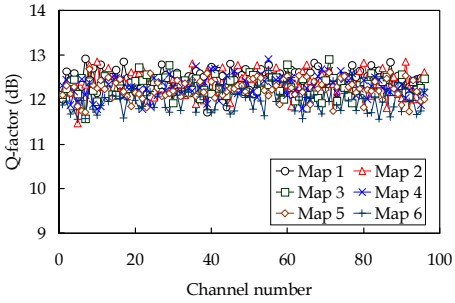

(B) +14 dBm

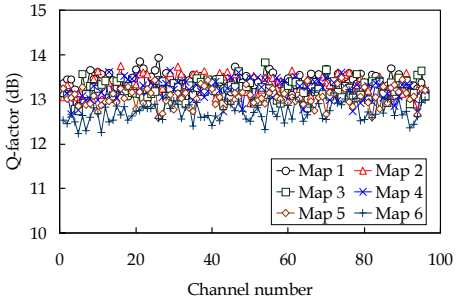

(C) +15 dBm

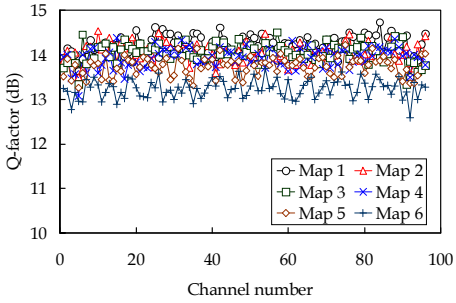

(D) +16 dBm

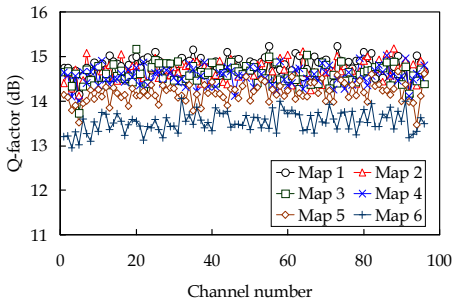

(E) +17 dBm

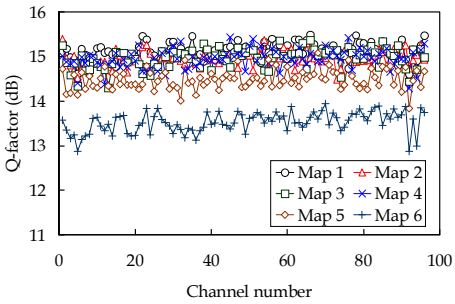

(F) +18 dBm

Fig. 18. Transmission performance of 96 channels as a function of the repeater output power

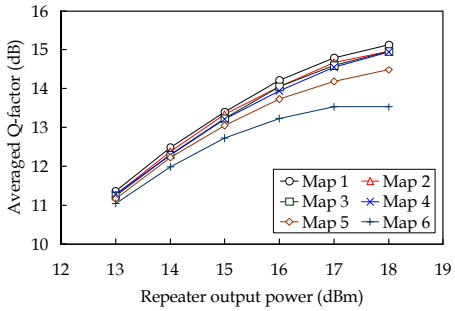

Fig. 19. Repeater output power dependency of different dispersion map

7. Conclusion

In this chapter, the transmission performance of the long-haul RZ-DPSK system with respect to the dispersion map design was discussed using the numerical simulations. The block type dispersion map could not realize better performance than the block-less type dispersion map either using the NZDSF or the DFF for the RZ-DPSK transmission. The reason of the performance degradation for the block type map was pointed out to be the SPM, and it was also confirmed experimentally (Wang & Taga, 2010). This proved the appropriateness of the numerical simulations for the long-haul RZ-DPSK based optical fibre communication system.

8. Acknowledgment

This work is supported partially by National Science Council 99-2221-E-110-030-MY3 and partially by Aim for the Top University Plan of the National Sun Yat-Sen University and Ministry of Education, Taiwan, R.O.C.

9. References

Agrawal, G. P. (2006). *Nonlinear Fiber Optics (Fourth Ed.)*, Academic Press, ISBN 978-0-12-369516-1, San Diego, California, USA

Bakhshi, B.; Manna, M.; Mohs, G.; Kovsh, D. I.; Lynch, R. L.; Vaa, M.; Golovchenko, E. A.; Patterson, W. W.; Anderson, W. T.; Corbett, P.; Jiang, S.; Sanders, M. M.; Li, H.; Harvey, G. T.; Lucero, A. & Abbott, S. M. (2004). First Dispersion-Flattened Transpacific Undersea System: From Design to Terabit/s Field Trial, *Journal of Lightwave Technology*, Vol.22, No.1, (January, 2004), pp. 233-241

Bergano, N. S.; Kerfoot, F. W. & Davidsion, C. R. (1993). "Margin measurements in optical amplifier system, *IEEE Photonics Technology Letters*, Vol.5, No.3, (March, 1993), pp. 304-306

Bergano, N. S. (2005). Wavelength division multiplexing in long-haul transoceanic transmission systems, *Journal of Lightwave Technology*, Vol.23, No.12, (December 2005), pp. 4125-4139

Bosco, G.; Carena, A.; Curri, V.; Gaudino, R.; Poggiolini, P. & Benedetto, S. (2000). Suppression of spurious tones induced by the split-step method in fiber systems simulation, *IEEE Photonics Technology Letters*, Vol.12, No.5, (May, 2000), pp. 489–491

Cai, J.-X.; Nissov, M.; Anderson, W.; Vaa, M.; Davidson, C. R.; Foursa, D. G.; Liu, L.; Cai, Y.; Lucero, A. J.; Patterson, W. W.; Corbett, P. C.; Pilipetskii, A. N. & Bergano, N. S. (2006). Long-haul 40 Gb/s RZ-DPSK transmission with long repeater spacing, *Proceedings of Optical Fiber Communication Conference*, paper OFD3, Anaheim, California, USA, March 5-10, 2006

Dupont, S.; Marmier, P.; Mouza, L. d.; Charlet, G. & Letellier, V. (2007). 70 x 10 Gbps (mixed RZ-OOK and RZDPSK) upgrade of a 7224km conventional 32 x 10 Gbps designed system, *Proceedings of European Conference of Optical Communication (ECOC)*, Paper 2.3.5, Berlin, Germany, September 16-20, 2007

Essiambre, R.-J. & Winzer, P. J. (2005). Fibre nonlinearities in electronically pre-distorted transmission, *Proceedings of European Conference of Optical Communication (ECOC)*, Paper Th3.2.2, Glasgow, Scotland, September 25-29, 2005

Inoue, T.; Ishida, K.; Tokura, T.; Shibano, E.; Taga, H.; Shimizu, K.; Goto, K. & Motoshima, K. (2004). 150km repeater span transmission experiment over 9,000klm, *Proceedings of European Conference of Optical Communication (ECOC)*, paper Th4.1.3, Stockholm, Sweden, September 5-9, 2004

Mohs, G. ; Anderson, W. T. & Golovchenko, E. A. (2007). A New Dispersion Map for Undersea Optical Communication Systems, *Proceedings of Optical Fiber Communication Conference and Exposition and The National Fiber Optic Engineers Conference*, paper JThA41, Anaheim, California, USA, March 25-30, 2007

OFS, Available from:<http://www.ofsoptics.com/resources/UWOceanFiber-fiber-115.pdf>

Personick, S. D. (1973). Receiver Design for Digital Fiber Optic Communication Systems, I & II, *The Bell System Technical Journal*, Vol.52, No.6, (July-August, 1973), pp. 843–886

Rasmussen, C.; Fjelde, T.; Bennike, J.; Liu, F.; Dey, S.; Mikkelsen, B.; Mamyshev, P.; Serbe, P.; Wagt, P. v. d.; Akasaka, Y.; Harris, D.; Gapontsev, D.; Ivshin, V. & Reeves-Hall, P. (2004). DWDM 40G Transmission Over Trans-Pacific Distance (10 000 km) Using CSRZ-DPSK, Enhanced FEC, and All-Raman-Amplified 100-km UltraWave Fiber Spans, *Journal of Lightwave Technology*, Vol.22, No.1, (January 2004), pp. 203-207

Taga, H.; Shu, S.-S.; Wu, J.-Y. & Shih, W.-T. (2007). A theoretical study of the effect of the dispersion map upon a long-haul RZ-DPSK transmission system, *IEEE Photonics Technology Letters*, Vol.19, No.24, (December, 2007), pp. 2060–2062

Taga, H.; Shu, S.-S.; Wu, J.-Y. & Shih, W.-T. (2008). A theoretical study of the effect of zero-crossing points within the dispersion map upon a long-haul RZ-DPSK system, *Optics Express*, Vol.16, No.9, (April, 2008), pp. 6163-6169

Taga, H. (2009). A theoretical investigation of the long-haul RZDPSK system performance using DFF and NZDSF, *Optics Express*, Vol.17, No.8, (April, 2009), pp. 6032-6037

Taga, H. & Chung, W.-H. (2010). Impact of dispersion map design upon transmission performance of long-haul RZDPSK system using dispersion flattened fiber, *Optics Express*, Vol.18, No.8, (April, 2010), pp. 8332-8337

Vaa, M.; Golovchenko, E. A.; Mohs, G.; Patterson, W. & Pillipetskii, A. (2004). Dense WDM RZ-DPSK transmission over transoceanic distances without use of periodic dispersion management, *Proceedings of European Conference of Optical Communication (ECOC)*, Paper Th4.4.4, Stockholm, Sweden, September 5-9, 2004

Wang, H. M. and Taga, H. (2010), An Experimental Study of XPM and SPM Upon a Long-Haul RZ-DSPK Transmission System With a Block-Type Dispersion Map, *Journal of Lightwave Technology*, Vol.28, No.22, (November, 2010), pp. 3220-3225

Wei, X.; Liu, X. & Xu, C. (2003). Numerical simulation of the SPM penalty in a 10-Gb/s RZ-DPSK system, *IEEE Photonics Technology Letters*, Vol.15, No.11, (November, 2003), pp. 1636–1638

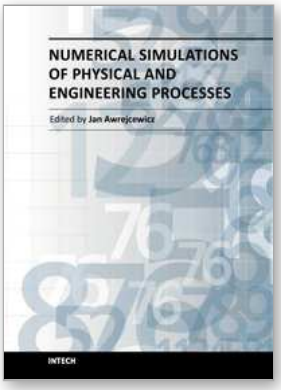

Numerical Simulations of Physical and Engineering Processes
Edited by Prof. Jan Awrejcewicz

ISBN 978-953-307-620-1
Hard cover, 594 pages
Publisher InTech
Published online 26, September, 2011
Published in print edition September, 2011

Numerical Simulations of Physical and Engineering Process is an edited book divided into two parts. Part I devoted to Physical Processes contains 14 chapters, whereas Part II titled Engineering Processes has 13 contributions. The book handles the recent research devoted to numerical simulations of physical and engineering systems. It can be treated as a bridge linking various numerical approaches of two closely inter-related branches of science, i.e. physics and engineering. Since the numerical simulations play a key role in both theoretical and application oriented research, professional reference books are highly needed by pure research scientists, applied mathematicians, engineers as well post-graduate students. In other words, it is expected that the book will serve as an effective tool in training the mentioned groups of researchers and beyond.

INTECH
open science | open minds

InTech Europe
University Campus STeP Ri
Slavka Krautzeka 83/A
51000 Rijeka, Croatia
Phone: +385 (51) 770 447
Fax: +385 (51) 686 166
www.intechopen.com

InTech China
Unit 405, Office Block, Hotel Equatorial Shanghai
No.65, Yan An Road (West), Shanghai, 200040, China
中国上海市延安西路65号上海国际贵都大饭店办公楼405单元
Phone: +86-21-62489820
Fax: +86-21-62489821